Joint Temporal Statistics of Interference in Decentralized Wireless Networks

Kapil Gulati, *Member, IEEE,* Brian L. Evans, *Fellow, IEEE,* and Srikathyayani Srikanteswara, *Member, IEEE*

***Abstract*—Characterizing interference statistics is central to the design and analysis of both physical layer and medium access control layer techniques to mitigate interference in a wireless network. The applicability of interference statistics, however, is limited by the assumptions adopted to derive the statistics in closed-form. Common assumptions for a decentralized wireless network include temporally independent user locations and an unbounded pathloss function. In this paper, we derive the joint temporal statistics of interference that capture the temporal correlation in the network along with the realistic assumption of a bounded pathloss function. The closed-form statistics are asymptotically exact for low tail probabilities, and match closely in simulations even when the tail probability is fairly high. The primary contributions are to (i) show that joint interference statistics follow a multivariate Gaussian mixture distribution under the assumption of a bounded pathloss function, and (ii) characterize the joint tail probability decay behavior for both bounded and unbounded pathloss functions.**

I. Introduction

Communication performance of a decentralized wireless network, such as a wireless ad hoc network, is limited due to interference. Characterizing the interference statistics is hence central to the design and analysis of a decentralized wireless network. Exact closed-form interference statistics, however, are only known under certain restrictive assumptions on user locations and the propagation environment. Common assumptions include: (i) temporally independent user locations that follow a Poisson point process (PPP), and (ii) an unbounded pathloss function $l(r) = r^{-\frac{\gamma}{2}}$, where r is the propagation distance and γ is the power pathloss exponent. Under these assumptions, the instantaneous statistics of interference follows a symmetric alpha stable distribution [1]–[6]. The assumption of temporally independent user locations limits the applicability of the statistics since it falls short of capturing the temporal correlation in the network [7]. An unbounded pathloss function, on the other hand, may limit the validity of the result by overestimating the effect of interference [8]. Nonetheless, these assumptions are common since they lead to closed-form interference statistics [1]–[3]. In this paper, we address these two limitations, while still deriving closed-form interference statistics.

Regarding assumption (i), user locations are often strongly correlated over time due to user mobility and transmission bursts that play out over a significantly slower time scale than contention and channel access. The temporal correlation in user locations results in temporally dependent interference, which in turn causes temporal correlation in network performance measures [7], [9]. The network model adopted in this paper spans the extremes of temporal independence to long-term temporal dependence in interference, thereby capturing random mobility and random queue size of users [3], [7]. For the network model adopted in this paper, and under the assumption of an unbounded pathloss function, the joint temporal statistics follow a multivariate symmetric alpha stable distribution – that is exact for Rayleigh faded user emissions, and accurately captures the tail probability of interference otherwise [3], [7]. Using a unified framework, we reestablish this result for completeness, while primarily focusing on a bounded pathloss function.

Regarding assumption (ii), an unbounded pathloss function is not realistic because it suggests that the received power is greater than the transmit power when $r < 1$. Further, the singularity at $r = 0$ affects the results by significantly overestimating the degradation in communication performance due to interference [8]. This motivates characterizing the interference for a more realistic bounded pathloss function. To the best of our knowledge, closed-form instantaneous or temporal statistics of interference under the assumption of a bounded pathloss function are not known.

In this paper, we derive closed-form interference statistics in a decentralized wireless network with temporally correlated user locations, under the assumptions of both unbounded $\left(l(r) = r^{-\frac{\gamma}{2}}\right)$ and bounded $\left(l(r) = \min\left(1, r^{-\frac{\gamma}{2}}\right)\right)$ pathloss functions. After giving the system model in Section II, Section III-A reestablishes that the joint temporal interference tails follow a multivariate symmetric alpha stable distribution under the assumption that $l(r) = r^{-\frac{\gamma}{2}}$. The primary contributions are to show that (i) joint temporal statistics of interference follow a multivariate Gaussian mixture distribution for $l(r) = \min\left(1, r^{-\frac{\gamma}{2}}\right)$ in Section III-B, and (ii) tail probability of interference $\mathbb{P}\left(\|\mathbf{I}\| > \beta\right)$ decays as $\Omega\left(e^{-\beta^2}\right)$ for a bounded pathloss function, and not $\Omega\left(\beta^{-\frac{4}{\gamma}}\right)$ as obtained under the assumption of an unbounded pathloss function, in Section IV. While the statistics are exact for asymptotically low tail

Manuscript submitted August 16, 2011; revised May 5, 2012; accepted August 1, 2012.

This research was supported by Intel Corporation.

K. Gulati is with Qualcomm Incorporated, San Diego, CA 92121, USA. He was with The University of Texas at Austin, TX 78712 USA during this research (e-mail: gulati.k@gmail.com).

B. L. Evans is with Wireless Networking and Communications Group, The University of Texas at Austin, TX 78712 USA (e-mail: gulati.k@gmail.com, bevans@ece.utexas.edu).

S. Srikanteswara is with Intel Corporation, Santa Clara, CA 95054 USA (e-mail: srikathyayani.srikanteswara@intel.com).

probabilities, Section V shows that simulations match closely even when the tail probability is fairly high. Section VI concludes the paper.

Throughout this paper, random variables are represented using boldface notation and deterministic variables are represented using non-boldface type.

II. System Model

Time is slotted at the symbol time scale. The locations of interferers, also referred to as nodes, are modeled using a spatial point process. As depicted in Fig. 1, a node is said to *emerge* at a particular time slot if it first starts to transmit at that time slot. The transmission burst is assumed to last for a random duration, termed as the *lifetime*. The random emerging time thus models the asynchronous nature of a decentralized network, and the random lifetime models the random queue size of users. All nodes transmitting at a given time slot are referred to as *active* nodes at that time slot. Thus at any time slot n, the set of active nodes is a union over the sets of nodes that emerged at a time slot $k \leq n$ and are still active at the time slot n. For simplicity in exposition, we assume that the transmission bursts are not subject to an additional channel access control protocol. The system model can be readily extended for a non-contention based access protocol (such as slotted-ALOHA) that induces an independent thinning of the point process governing the node locations.

Emerging nodes at any time slot k are assumed to be spatially distributed according to a homogeneous PPP $\mathbf{\Pi}^{(k)} = \left\{\left(\mathbf{R}_i^{(k)}, \mathbf{L}_i^{(k)}\right), i \geq 1\right\}$ with intensity λ. Here $\mathbf{R}_i^{(k)}$ is the random location of the node i that first emerged at time k, and $\mathbf{L}_i^{(k)} \geq 1$ is the random number of time slots (lifetime) it intends to be active. The point process of active nodes at time slot n can then be represented as $\mathbf{\Xi}_n = \bigcup_{k=-\infty}^{n} \mathbf{\Xi}_{k,n}$, where $\mathbf{\Xi}_{k,n} = \left\{\mathbf{R} : (\mathbf{R}, \mathbf{L}) \in \mathbf{\Pi}^{(k)}, \mathbf{L} \geq n-k+1\right\}$ is the set of interferers that first emerged at time slot k and are still active at time n. Note that for $n < k$, $\mathbf{\Xi}_{k,n}$ is an empty set. The interference at any time slot n can then be represented as

$$\mathbf{I}_n = \sum_{k=-\infty}^{n} \mathbf{I}_{k,n} = \sum_{k=-\infty}^{n} \sum_{\mathbf{R}_i \in \mathbf{\Xi}_{k,n}} l(\mathbf{r}_i)\mathbf{h}_i(n)\mathbf{B}_i(n) \exp\left(\boldsymbol{\phi}_i(n)+\boldsymbol{\theta}_i(n)\right) \quad (1)$$

where $\mathbf{I}_{k,n}$ is the sum interference at time slot n due to interferers that first emerged at time slot k, i is the interferer index, $\mathbf{r}_i = \|\mathbf{R}_i\|$ are the random distances of active interferers from the receiver, $\mathbf{B}_i(n)e^{j\boldsymbol{\phi}_i(n)}$ are the narrowband interferer emissions from interferer i at time slot n, $\mathbf{h}_i(n)e^{j\boldsymbol{\theta}_i(n)}$ is the fast fading experienced by the interferer emissions, and $l(\cdot)$ is the pathloss function that models the decay of transmit power with distance. Random variables $\mathbf{B}_i(n), \mathbf{h}_i(n), \boldsymbol{\phi}_i(n), \boldsymbol{\theta}_i(n)$ are each assumed to be *i.i.d.* for every interferer i and time slot n. At the symbol time scale, the random amplitude and phase are typically uncorrelated over time, but may still be temporally dependent. The assumption of temporally *i.i.d.* amplitude and phase, however, is made for mathematical tractability and does not affect the large scale trends (i.e., decay rate of tail probability) in the results. Similarly, slow fading channel variations (e.g., shadowing) are not included for mathematical tractability as it does not affect the large scale trends in the results [7]. Assuming the actual emerging time of the interferers to be uniformly distributed between two consecutive time slots, $\boldsymbol{\phi}_i(n)$ and $\boldsymbol{\theta}_i(n)$ can be assumed to be uniformly distributed on $[0, 2\pi]$.

III. Joint Statistics of Interference

Let $\bar{\mathbf{I}}_{k,1:n} = \left\{\mathbf{I}_{k,1}^{(I)}, \mathbf{I}_{k,1}^{(Q)}, \cdots, \mathbf{I}_{k,n}^{(I)}, \mathbf{I}_{k,n}^{(Q)}\right\}$ denote the vector of in-phase and quadrature phase components on interference at time slots 1 through n due to nodes that emerged at time slot k. Similarly, let $\bar{\mathbf{I}}_{1:n} = \left\{\mathbf{I}_1^{(I)}, \mathbf{I}_1^{(Q)}, \cdots, \mathbf{I}_n^{(I)}, \mathbf{I}_n^{(Q)}\right\}$ denote the vector of in-phase and quadrature phase components of interference at time slots 1 through n due to nodes that emerged anytime until slot n. Further, let $\overline{\omega}_{1:n} = \left\{\omega_1^{(I)}, \omega_1^{(Q)}, \cdots, \omega_n^{(I)}, \omega_n^{(Q)}\right\}$ denote the vector of frequency variables. We consider the nodes to be distributed over disc of radius R, denoted as $b(0,R)$, and take the limit on the joint distribution as $R \to \infty$. Using (1) and noting that the underlying PPP of emerging nodes at any time slot k is mutually independent for all k, the joint characteristic function of $\bar{\mathbf{I}}_{1:n}$ can be expressed as

$$\mathbf{\Phi}_{\bar{\mathbf{I}}_{1:n}}(\overline{\omega}_{1:n}) = \prod_{k=-\infty}^{n} \mathbf{\Phi}_{\bar{\mathbf{I}}_{k,1:n}}(\overline{\omega}_{1:n}) \quad (2)$$

where $\mathbf{\Phi}_{\bar{\mathbf{I}}_{k,1:n}}(\overline{\omega}_{1:n})$ is the joint characteristic function of $\bar{\mathbf{I}}_{k,1:n}$. Using (1), the joint characteristic function of $\bar{\mathbf{I}}_{k,1:n}$ is given as

$$\mathbf{\Phi}_{\bar{\mathbf{I}}_{k,1:n}}(\overline{\omega}_{1:n}) = \mathbb{E}\left\{\exp\left(j\sum_{m=1}^{n}\left(\omega_m^{(I)}\mathbf{I}_{k,m}^{(I)} + \omega_m^{(Q)}\mathbf{I}_{k,m}^{(Q)}\right)\right)\right\} \quad (3)$$

$$= \mathbb{E}\left\{\exp\left(j\sum_{m=1}^{n}|\omega_m| \sum_{\mathbf{R}_i \in \mathbf{\Xi}_{k,m}} l(\mathbf{r}_i)\mathbf{h}_i(m)\mathbf{B}_i(m)\times \cos\left(\boldsymbol{\phi}_i(m)+\boldsymbol{\theta}_i(m)+\boldsymbol{\phi}_{\omega_m}\right)\right)\right\} \quad (4)$$

$$= \mathbb{E}\left\{\exp\left(j\sum_{m=1}^{n}|\omega_m| \sum_{(\mathbf{R}_i,\mathbf{L}_i)\in\mathbf{\Pi}^{(k)}} l(\mathbf{r}_i)\mathbf{h}_i(m)\mathbf{B}_i(m)\times \cos\left(\boldsymbol{\phi}_i(m)+\boldsymbol{\theta}_i(m)+\boldsymbol{\phi}_{\omega_m}\right)\mathbf{1}\left(\mathbf{L}_i \geq m-k+1>0\right)\right)\right\} \quad (5)$$

$$= \exp\left(\lambda\pi R^2\left(-1+\mathbb{E}\left\{\exp\left(j\sum_{m=1}^{n}|\omega_m|\, l(\mathbf{r}_i)\mathbf{h}(m)\mathbf{B}(m)\times \cos\left(\boldsymbol{\phi}(m)+\boldsymbol{\theta}(m)+\boldsymbol{\phi}_{\omega_m}\right)\mathbf{1}\left(\mathbf{L} \geq m-k+1>0\right)\right)\right\}\right)\right) \quad (6)$$

where $|\omega_m| = \sqrt{\left(\omega_m^{(I)}\right)^2 + \left(\omega_m^{(Q)}\right)^2}$, $\phi_{\omega_m} = \tan^{-1}\left(\frac{\omega_m^{(Q)}}{\omega_m^{(I)}}\right)$, $\mathbf{1}(\cdot)$ is the indicator function, and the expectation in (6) is with respect to the set of random variables

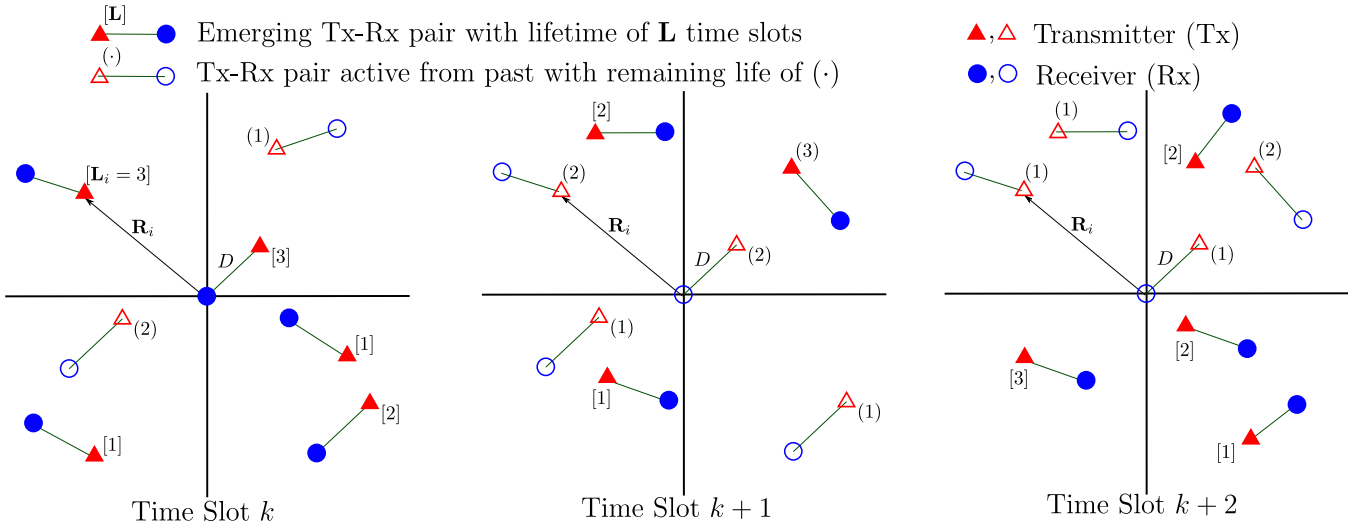

Fig. 1: Network model where nodes can emerge at any time slot and are active for a random number of time slots ($= \mathbf{L}$).

$\{\mathbf{r}, \mathbf{L}, \mathbf{h}(m), \mathbf{B}(m), \boldsymbol{\phi}(m), \boldsymbol{\theta}(m)\}$. Equation (5) holds since $\boldsymbol{\Xi}_{k,m} = \left\{\mathbf{R} : (\mathbf{R}, \mathbf{L}) \in \boldsymbol{\Pi}^{(k)}, \mathbf{L} \geq m-k+1\right\}$ for $m \geq k$, and is an empty set for $m < k$. Equation (6) is derived using the probability generating functional (PGFL) of a homogeneous PPP [10] and holds since the node emissions, node lifetime, and fading are each assumed to be *i.i.d.* across time slots and nodes. Note that the expectation in (6) is conditioned such that the node locations are uniformly distributed over $b(0, R)$ [6], [10]. Using the identity

$$e^{ja\cos(\phi)} = \sum_{l=0}^{\infty} j^l \boldsymbol{\epsilon}_l J_l(a)\cos(l\phi) \tag{7}$$

where $\boldsymbol{\epsilon}_0 = 1$, $\boldsymbol{\epsilon}_l = 2$ for $l \geq 1$, and $J_l(\cdot)$ denotes the Bessel function of order l, the log-characteristic function $\psi_{\bar{\mathbf{I}}_{k,1:n}}(\overline{\omega}_{1:n}) \triangleq \log \Phi_{\bar{\mathbf{I}}_{k,1:n}}(\overline{\omega}_{1:n})$ can be expressed as

$$\begin{aligned}
&\psi_{\bar{\mathbf{I}}_{k,1:n}}(\overline{\omega}_{1:n}) \\
&= \lambda\pi R^2\Bigg[-1+\mathbb{E}\Bigg\{\prod_{m=1}^{n}\Bigg(\sum_{l=0}^{\infty} j^l \boldsymbol{\epsilon}_l J_l\Big(|\omega_m| l(\mathbf{r})\mathbf{h}(m)\mathbf{B}(m)\times \\
&\mathbf{1}\left(\mathbf{L}\geq m-k+1>0\right)\Big)\cos\left(l\left(\boldsymbol{\phi}(m)+\boldsymbol{\theta}(m)+\boldsymbol{\phi}_{\omega_m}\right)\right)\Bigg)\Bigg\}\Bigg] \qquad (8)\\
&= \lambda\pi R^2\Bigg[-1+\mathbb{E}\Bigg\{\prod_{m=1}^{n} J_0\Big(|\omega_m| l(\mathbf{r})\mathbf{h}(m)\mathbf{B}(m)\times \\
&\qquad\qquad \mathbf{1}\left(\mathbf{L}\geq m-k+1>0\right)\Big)\Bigg\}\Bigg] \qquad (9)\\
&= \lambda\pi R^2\Bigg[\sum_{s=1}^{n}\overline{F}_{\mathbf{L}}^{(k,n)}(s)\Bigg(-1+ \\
&\qquad \mathbb{E}\Bigg\{\prod_{m=\max(1,k)}^{s} J_0\left(|\omega_m| l(\mathbf{r})\mathbf{h}(m)\mathbf{B}(m)\right)\Bigg\}\Bigg)\Bigg] \qquad (10)
\end{aligned}$$

where

$$\overline{F}_{\mathbf{L}}^{(k,n)}(s) = \begin{cases} 0 & s < k, \\ \mathbb{P}(\mathbf{L} = s-k+1) & k \leq s < n, \\ \mathbb{P}(\mathbf{L} \geq s-k+1) & s = n. \end{cases} \tag{11}$$

The expectation in (8) is with respect to the set of random variables $\{\mathbf{r}, \mathbf{L}, \mathbf{h}(m), \mathbf{B}(m), \boldsymbol{\phi}(m), \boldsymbol{\theta}(m)\}$. Equation (9) involves expanding the expectation over $\boldsymbol{\phi}(m)$ and $\boldsymbol{\theta}(m)$, where $\boldsymbol{\phi}(m), \boldsymbol{\theta}(m)$ are mutually independent and uniformly distributed in $[0, 2\pi]$ and *i.i.d.* across time slots m, and noting that $\mathbb{E}_{\boldsymbol{\phi}(m),\boldsymbol{\theta}(m)}\{\cos\left(l(\boldsymbol{\phi}(m)+\boldsymbol{\theta}(m)+\phi_{\omega_m})\right)\} = 0$ for $l \geq 1$ for all time slots m. Equation (10) is derived by expanding the expectation over lifetime random variable $\mathbf{L}$. The expectation in (10) is thus with respect to the set of random variables $\{\mathbf{r}, \mathbf{h}(m), \mathbf{B}(m)\}$. To further simplify (10), we express it as

$$\psi_{\bar{\mathbf{I}}_{k,1:n}}(\overline{\omega}_{1:n}) = \lambda\pi\left[\sum_{s=1}^{n}\overline{F}_{\mathbf{L}}^{(k,n)}(s)\Upsilon_{(k,s)}(\overline{\omega}_{1:n})\right] \tag{12}$$

where for any parameters $\{k, s\}$,

$$\begin{aligned}
&\Upsilon_{(k,s)}(\overline{\omega}_{1:n}) \\
&= \lim_{R\to\infty} R^2\Bigg(-1+ \\
&\qquad \mathbb{E}\Bigg\{\prod_{m=\max(1,k)}^{s} J_0\left(|\omega_m| l(\mathbf{r})\mathbf{h}(m)\mathbf{B}(m)\right)\Bigg\}\Bigg) \qquad (13)\\
&= \lim_{R\to\infty} R^2\Bigg(-1+ \\
&\qquad \int_0^R \prod_{m=\max(1,k)}^{s} \mathbb{E}_{\mathbf{h},\mathbf{B}}\left\{J_0\left(|\omega_m| l(r)\mathbf{h}\mathbf{B}\right)\right\}\frac{2r}{R^2}dr\Bigg) \qquad (14)\\
&= -\int_0^{\infty}\frac{\partial}{\partial r}\Bigg(\prod_{m=\max(1,k)}^{s} \mathbb{E}_{\mathbf{h},\mathbf{B}}\left\{J_0\left(|\omega_m| l(r)\mathbf{h}\mathbf{B}\right)\right\}\Bigg) r^2 dr. \\
&\qquad\qquad (15)
\end{aligned}$$

Equation (14) is derived by expanding the expectation over $\mathbf{r}$ in (13) and noting that $\mathbf{h}(m)$ and $\mathbf{B}(m)$ are each *i.i.d.* across time slots m. Equation (15) involves integrating (14) by parts and noting that

$\lim_{R\to\infty} R^2\left(-1+\prod_{m=\max(1,k)}^{s}\mathbb{E}_{\mathbf{h},\mathbf{B}}\left\{J_0\left(|\omega_m|\, l(R)\mathbf{hB}\right)\right\}\right)=0$ if $\lim_{R\to\infty} Rl(R)=0$. The condition $\lim_{R\to\infty} Rl(R)=0$ is satisfied when $\gamma>2$, since the power-law decay $l(r)=r^{-\frac{\gamma}{2}}$ is accurate when $r\gg 1$ [8].

To the best of our knowledge, exact evaluation of (15) for any general distribution of the random variable $\mathbf{hB}$ and a general power pathloss function $l(r)$ is not possible. Under the assumption that $\mathbb{E}_{\mathbf{h},\mathbf{B}}(\mathbf{h}^2\mathbf{B}^2)$ is finite, we invoke the following identity to simplify (15) [11]:

$$\mathbb{E}_{\mathbf{h},\mathbf{B}}\left\{J_0\left(|\omega_m|\, l(r)\mathbf{hB}\right)\right\}=e^{-\frac{|\omega_m|^2(l(r))^2\mathbb{E}_{\mathbf{h},\mathbf{B}}\left\{\mathbf{h}^2\mathbf{B}^2\right\}}{4}}\times \left(1+\mathbf{\Lambda}(|\omega_m|)\right) \quad (16)$$

where $\mathbf{\Lambda}(|\omega_m|)$ indicates a correction term with the lowest exponent in $|\omega_m|$ of four and is given by

$$\mathbf{\Lambda}(|\omega_m|)=\sum_{k=2}^{\infty}\frac{\left(\mathbb{E}_{\mathbf{Z}}\{\mathbf{Z}\}\right)^k|\omega_m|^{2k}\left(l(r)\right)^{2k}}{2^{2k}k!}\times \mathbb{E}_{\mathbf{Z}}\left\{{}_1F_1\left(-k;1;\frac{\mathbf{Z}}{\mathbb{E}_{\mathbf{Z}}\{\mathbf{Z}\}}\right)\right\} \quad (17)$$

where the random variable $\mathbf{Z}=\mathbf{h}^2\mathbf{B}^2$, and ${}_1F_1\left(a;b;x\right)$ is the confluent hypergeometric function of the first kind. Also $\mathbf{\Lambda}(|\omega_m|)=O\left(|\omega_m|^4\right)$ as $|\omega_m|\to 0$.

From Fourier analysis, the behavior of the characteristic function for $|\overline{\omega}|$ in the neighborhood of zero governs the tail probability of the random envelope. Thus to accurately model the tails, we approximate $\mathbf{\Lambda}(|\omega_m|)\ll 1$ for $|\omega_m|$ in the neighborhood of zero $\forall m\in[1,n]$, such that (15) reduces to

$$\Upsilon_{(k,s)}\left(\overline{\omega}_{1:n}\right) \approx -\int_0^{\infty}\frac{\partial}{\partial r}\left(e^{-\frac{\left(\sum_{m=\max(1,k)}^{s}|\omega_m|^2\right)(l(r))^2\mathbb{E}_{\mathbf{h},\mathbf{B}}\left\{\mathbf{h}^2\mathbf{B}^2\right\}}{4}}\right)r^2dr. \quad (18)$$

When $\mathbf{hB}$ is Rayleigh distributed, e.g., for constant amplitude modulated transmissions in Rayleigh fading environment, then $\mathbf{\Lambda}(|\omega_m|)=0$ and the expression in (18) is exact. We now simplify $\Upsilon_{(k,s)}\left(\overline{\omega}_{1:n}\right)$ for the following bounded and unbounded pathloss functions.

A. Unbounded Pathloss Function $l(r)=r^{-\frac{\gamma}{2}}$

Under the assumption of an unbounded pathloss function $l(r)=r^{-\frac{\gamma}{2}}$, (18) reduces to

$$\Upsilon_{(k,s)}\left(\overline{\omega}_{1:n}\right) =-\left[\left(\sum_{m=\max(1,k)}^{s}|\omega_m|^2\right)\frac{\mathbb{E}\left\{\mathbf{h}^2\mathbf{B}^2\right\}}{4}\right]^{\frac{2}{\gamma}}\Gamma\left(1-\frac{2}{\gamma}\right) \quad (19)$$

where $\Gamma(\cdot)$ denotes the Gamma function [7]. Substituting (19) in (12), and then using (2), the log-characteristic function of $\overline{\mathbf{I}}_{1:n}$ can be expressed as

$$\psi_{\overline{\mathbf{I}}_{1:n}}\left(\overline{\omega}_{1:n}\right) =-\overline{\rho}\sum_{k=-\infty}^{n}\left[\sum_{s=1}^{n}\overline{F}_{\mathbf{L}}^{(k,n)}(s)\left(\sqrt{\sum_{m=\max(1,k)}^{s}|\omega_m|^2}\right)^{\frac{4}{\gamma}}\right] \quad (20)$$

$$=-\overline{\rho}\sum_{i_1=1}^{n}\sum_{i_2=i_1}^{n}\overline{N}_{\mathbf{L}}^{(n)}(i_1,i_2)\left(\sqrt{\sum_{m=i_1}^{i_2}|\omega_m|^2}\right)^{\frac{4}{\gamma}} \quad (21)$$

where $\overline{\rho}=\left(\frac{\mathbb{E}_{\mathbf{h},\mathbf{B}}\left\{\mathbf{h}^2\mathbf{B}^2\right\}}{4}\right)^{\frac{2}{\gamma}}\Gamma\left(1-\frac{2}{\gamma}\right)$ and $\overline{N}_{\mathbf{L}}^{(n)}(i_1,i_2)=\lambda\pi\times\begin{cases}\overline{F}_{\mathbf{L}}^{(i_1,n)}(i_2) & i_1\neq 1,\\ \sum_{i=0}^{\infty}\overline{F}_{\mathbf{L}}^{(i_1,n+i)}(i_2+i) & i_1=1.\end{cases}$

Equation (21) corresponds to a $2n$-dimensional symmetric alpha stable vector with characteristic exponent $\alpha=\frac{4}{\gamma}$ [12]. To gain intuition into the above expression, we express $\overline{N}_{\mathbf{L}}^{(n)}(i_1,i_2)$ in matrix form with respect to the lifetime probabilities as (22). Using (21), we note that $\overline{N}_{\mathbf{L}}^{(n)}(i_1,i_2)$ contributes to the joint log-characteristic function in the dimensions corresponding to $\left\{\omega_{i_1}^{(I)},\omega_{i_1}^{(Q)},\cdots,\omega_{i_2}^{(I)},\omega_{i_2}^{(Q)}\right\}$. Thus $\overline{N}_{\mathbf{L}}^{(n)}(i_1,i_2)/\pi$ is the density of interferers that first emerged at time slot i_1 (or before when $i_1=1$, that corresponds to the first row) and are active exactly until time slot i_2 (or beyond for $i_2=n$, that corresponds to the last column).

B. Bounded Pathloss Function $l(r)=\min\left(1,r^{-\frac{\gamma}{2}}\right)$

For a bounded pathloss function $l(r)=\min\left(1,r^{-\frac{\gamma}{2}}\right)$, (18) can be expressed as

$$\Upsilon_{(k,s)}\left(\overline{\omega}_{1:n}\right) =-\sum_{k=1}^{\infty}\frac{\left(-\left(\sum_{m=\max(1,k)}^{s}|\omega_m|^2\right)\mathbb{E}_{\mathbf{h},\mathbf{B}}\left\{\mathbf{h}^2\mathbf{B}^2\right\}\right)^k}{4^kk!}\times \int_0^{\infty}\left(\frac{\partial\left(l(r)\right)^{2k}}{\partial r}\right)r^2dr \quad (23)$$

$$=\sum_{k=1}^{\infty}\frac{\left(-\left(\sum_{m=\max(1,k)}^{s}|\omega_m|^2\right)\mathbb{E}_{\mathbf{h},\mathbf{B}}\left\{\mathbf{h}^2\mathbf{B}^2\right\}\right)^k}{4^kk!}\frac{k\gamma}{k\gamma-2}. \quad (24)$$

The multiplicative factor $\frac{k\gamma}{k\gamma-2}$ in (24) prevents the log-characteristic function to be expressed in closed-form. Identical to the approach used in [6] for networks with guard zones, we approximate $\frac{k\gamma}{k\gamma-2}$ as $1+\eta e^{\beta k}$. The parameters η and β are chosen to minimize the weighted mean squared error (WMSE)

$$\{\eta,\beta\}=\arg\min_{\eta,\beta}\sum_{k=1}^{\infty}\left(\frac{k\gamma}{k\gamma-2}-\left(1+\eta e^{\beta k}\right)\right)^2u(k) \quad (25)$$

where $u(k)$ are the weights. The weights should be chosen such that penalty of error is large when k is small, since it affects the coefficients of terms with lower order exponents of $|\overline{\omega}|$. Equation (25) is an unconstrained nonlinear optimization problem that can be solved using numerical techniques such as

$$\overline{N}_{\mathbf{L}}^{(n)}(i_1,i_2)=\lambda\pi\begin{bmatrix}\mathbb{P}\left(\mathbf{L}\geq 1\right) & \mathbb{P}\left(\mathbf{L}\geq 2\right) & \mathbb{P}\left(\mathbf{L}\geq 3\right) & \cdots & \mathbb{P}\left(\mathbf{L}\geq n-1\right) & \sum\limits_{k=n}^{\infty}\mathbb{P}\left(\mathbf{L}\geq k\right)\\ 0 & \mathbb{P}\left(\mathbf{L}=1\right) & \mathbb{P}\left(\mathbf{L}=2\right) & \cdots & \mathbb{P}\left(\mathbf{L}=n-2\right) & \mathbb{P}\left(\mathbf{L}\geq n-1\right)\\ 0 & 0 & \mathbb{P}\left(\mathbf{L}=1\right) & \cdots & \mathbb{P}\left(\mathbf{L}=n-3\right) & \mathbb{P}\left(\mathbf{L}\geq n-2\right)\\ \vdots & \vdots & \ddots & \ddots & \vdots & \vdots\\ 0 & 0 & 0 & \cdots & \mathbb{P}\left(\mathbf{L}=1\right) & \mathbb{P}\left(\mathbf{L}\geq 2\right)\\ 0 & 0 & 0 & \cdots & 0 & \mathbb{P}\left(\mathbf{L}\geq 1\right)\end{bmatrix}. \tag{22}$$

quasi-Newton methods [13]. Using the weights $u(k)=e^{-k}$, $\{\eta,\beta\}$ can be estimated with an associated WMSE of less than 10^{-3} in a meaningful range of the pathloss exponent $(2<\gamma\leq 8)$ [6]. By approximating $\frac{k\gamma}{k\gamma-2}$ as $1+\eta e^{\beta k}$ using (25) for $k\geq 1$, (24) can be expressed as

$$\Upsilon_{(k,s)}\left(\overline{\omega}_{1:n}\right)=-(1+\eta)+e^{-\frac{\mathbb{E}_{\mathbf{h},\mathbf{B}}\left\{\mathbf{h}^2\mathbf{B}^2\right\}\sum\limits_{m=\max(1,k)}^{s}|\omega_m|^2}{4}}+\eta e^{-\frac{\mathbb{E}_{\mathbf{h},\mathbf{B}}\left\{\mathbf{h}^2\mathbf{B}^2\right\}e^{\beta}\sum\limits_{m=\max(1,k)}^{s}|\omega_m|^2}{4}}. \tag{26}$$

This approach can be generalized for any bounded pathloss function $l(r)$ by replacing $\frac{k\gamma}{k\gamma-2}$ with $\int\limits_0^{\infty}\left(\frac{\partial(l(r))^{2k}}{\partial r}\right)r^2dr$ in (25). Using (12), (26), and (2), the log-characteristic function of $\bar{\mathbf{I}}_{1:n}$ becomes

$$\psi_{\bar{\mathbf{I}}_{1:n}}\left(\overline{\omega}_{1:n}\right)=\sum_{i_1=1}^{n}\sum_{i_2=i_1}^{n}N(i_1,i_2)\Bigg(-(1+\eta)+e^{-\frac{\mathbb{E}\left\{\mathbf{h}^2\mathbf{B}^2\right\}\sum\limits_{m=i_1}^{i_2}|\omega_m|^2}{4}}+\eta e^{-\frac{\mathbb{E}\left\{\mathbf{h}^2\mathbf{B}^2\right\}e^{\beta}\sum\limits_{m=i_1}^{i_2}|\omega_m|^2}{4}}\Bigg). \tag{27}$$

Equation (27) corresponds to the log-characteristic function of a multivariate Gaussian mixture distribution. The joint characteristic function, if expressed directly using (27), involves many summations. Each exponential term in the log-characteristic function leads to a Gaussian mixture series expression in the joint characteristic function. Using (27), and truncating each of the Gaussian mixture series summation to N_T terms, the joint characteristic function can be expressed in a more concise form as

$$\mathbf{\Phi}_{\bar{\mathbf{I}}_{1:n}}\left(\overline{\omega}_{1:n}\right)\approx\left(e^{-(1+\eta)\sum\limits_{i_1=1}^{n}\sum\limits_{i_2=i_1}^{n}\overline{N}_{\mathbf{L}}^{(n)}(i_1,i_2)}\right)\times\sum_{i=1}^{(N_T)^{2n!}}\overline{p}(i)e^{-\sum\limits_{m=1}^{n}\frac{|\omega_m|^2\overline{\sigma}_m^2(i)}{2}} \tag{28}$$

where $\overline{p}=\bigotimes\limits_{i_1=1}^{n}\left(\bigotimes\limits_{i_2=i_1}^{n}k_{i_1,i_2}\right)$ is a $(N_T)^{2n!}\times 1$ length vector of mixture probabilities. Here $k_{i_1,i_2}=k_{i_1,i_2}^{(1)}\bigotimes k_{i_1,i_2}^{(2)}$, and for $i_2\geq i_1$,

$$k_{i_1,i_2}^{(1)},k_{i_1,i_2}^{(2)}=e^{-(1+\eta)\sum\limits_{i_1=1}^{n}\sum\limits_{i_2=i_1}^{n}\overline{N}_{\mathbf{L}}^{(n)}(i_1,i_2)}\times\left\{\begin{bmatrix}\frac{\left(\overline{N}_{\mathbf{L}}^{(n)}(i_1,i_2)\right)^0}{0!}\\ \vdots\\ \frac{\left(\overline{N}_{\mathbf{L}}^{(n)}(i_1,i_2)\right)^{N_T-1}}{(N_T-1)!}\end{bmatrix},\begin{bmatrix}\frac{\left(\eta\overline{N}_{\mathbf{L}}^{(n)}(i_1,i_2)\right)^0}{0!}\\ \vdots\\ \frac{\left(\eta\overline{N}_{\mathbf{L}}^{(n)}(i_1,i_2)\right)^{N_T-1}}{(N_T-1)!}\end{bmatrix}\right\}. \tag{29}$$

Similarly $\overline{\sigma}_m^2=\bigoplus\limits_{i_1=1}^{n}\left(\bigoplus\limits_{i_2=i_1}^{n}t_{i_1,i_2}^{(m)}\right)$ are a $(N_T)^{2n!}\times 1$ length vector of mixture variances corresponding to the m^{th} component in the joint distribution. Here $t_{i_1,i_2}^{(m)}=t_{i_1,i_2}^{(m,1)}\bigoplus t_{i_1,i_2}^{(m,2)}$, and

$$t_{i_1,i_2}^{(m,1)},t_{i_1,i_2}^{(m,2)}=\frac{\mathbb{E}_{\mathbf{h},\mathbf{B}}\left\{\mathbf{h}^2\mathbf{B}^2\right\}}{2}\times\begin{cases}\begin{bmatrix}0\\ \vdots\\ N_T-1\end{bmatrix},\begin{bmatrix}e^{\beta}\times 0\\ \vdots\\ e^{\beta}\times(N_T-1)\end{bmatrix} & \text{if } i_1\leq m\leq i_2,\\ \overline{0},\overline{0} & \text{otherwise.}\end{cases} \tag{30}$$

where $\overline{0}$ represents a $N_T\times 1$ zero vector. Expressing the joint characteristic function of $\bar{\mathbf{I}}_{1:n}$ as (28) is helpful in recognizing the multivariate Gaussian mixture form. The approximation in (28) can be made arbitrarily accurate by increasing N_T.

IV. Joint Tail Probability of Interference Amplitude

In this section, we provide the results for the joint tail probability of interference given as

$$\mathbb{P}(\Delta>n)=\mathbb{P}\left(\|\mathbf{I}_1\|>\beta_1,\|\mathbf{I}_2\|>\beta_2,\cdots,\|\mathbf{I}_n\|>\beta_n\right). \tag{31}$$

Equation (31) directly relates to an joint outage event where the signal-to-interference ratio falls below the detection threshold for n consecutive time slots [7], [14].

A. Unbounded pathloss function $l(r)=r^{-\frac{\gamma}{2}}$

For $l(r)=r^{-\frac{\gamma}{2}}$, the multivariate symmetric alpha stable distribution in (21) is shown to accurately model the joint interference tails. For $\beta_1,\cdots,\beta_n$ large, the joint amplitude tails corresponding to the joint characteristic function (21) was derived in [7], and is given as

$$\mathbb{P}(\Delta>n)\approx\left(\sqrt{\sum_{i=1}^{n}\beta_i^2}\right)^{-\alpha}2^{\alpha}\overline{\rho}\overline{N}_{\mathbf{L}}^{(n)}(1,n)\frac{\Gamma\left(1+\frac{\alpha}{2}\right)}{\Gamma\left(1-\frac{\alpha}{2}\right)}. \tag{32}$$

B. Bounded pathloss function $l(r) = \min\left(1, r^{-\frac{\gamma}{2}}\right)$

For $l(r) = \min\left(1, r^{-\frac{\gamma}{2}}\right)$, the multivariate Gaussian mixture distribution in (28) is shown to accurately model the joint interference tails. Using (28), the joint amplitude tails are given as

$$\mathbb{P}(\Delta > n) \approx \left(e^{-(1+\eta)\sum_{i_1=1}^{n}\sum_{i_2=i_1}^{n} \overline{N}_{\mathbf{L}}^{(n)}(i_1,i_2)} \right) \times \sum_{i=1}^{(N_T)^{2n!}} \overline{p}(i) e^{-\sum_{m=1}^{n} \frac{\beta_m^2}{2\overline{\sigma}_m^2(i)}}. \quad (33)$$

Note that the right hand sides in (32) and (33) are the dominant terms of the joint tail probability for unbounded and bounded pathloss functions, respectively. Thus a bounded pathloss function $l(r) = \min\left(1, r^{-\frac{\gamma}{2}}\right)$ leads to $\Omega\left(e^{-\beta^2}\right)$ decay in tail probability, as opposed to $\Omega\left(\beta^{-\alpha}\right)$ under the assumption of an unbounded pathloss function.

V. Simulation Results

Using the physical model discussed in Section II, we apply Monte Carlo numerical techniques to simulate the interference observed at any typical receiver in a decentralized wireless network. Accuracy of the interference distributions is established by comparing the empirical and analytical joint tail probability for both bounded and unbounded pathloss functions. The network model parameters used in numerical simulations are: $\gamma = 4, \lambda = 0.005, \mathbf{B} = 10$, and the lifetime ($\mathbf{L}$) of a typical node is assumed to follow a truncated Poisson distribution over $[1, L_{\max} = 10]$ time slots and a mean of $\overline{L} = 5$ time slots, given as

$$\mathbf{L} \sim \left(\sum_{l=1}^{L_{\max}} \frac{\overline{L}^l}{l!} \right)^{-1} \frac{\overline{L}^l}{l!} \qquad l = 1, \cdots, L_{\max}. \quad (34)$$

Figs. 2 and 3 show the joint tail probability of interference over $n = \{2, 3\}$ consecutive time slots in the presence of Rayleigh $\left(\mathbf{h} \sim \text{Rayleigh}\left(\frac{1}{\sqrt{2}}\right)\right)$ and Nakagami $\left(\mathbf{h}^2 \sim \text{Gamma}(0.5, 2)\right)$ fading, respectively. The multivariate symmetric alpha stable and the multivariate Gaussian mixture distributions can be seen to accurately model the tail probability of interference for unbounded $\left(l(r) = r^{-\frac{\gamma}{2}}\right)$ and bounded $\left(l(r) = \min\left(1, r^{-\frac{\gamma}{2}}\right)\right)$ pathloss functions, respectively. Further, the correspondence in tail probability is more accurate for Rayleigh fading since $\mathbf{\Lambda}(|\omega_m|) = 0$ when $\mathbf{hB} \sim$Rayleigh, and thus (18) is exact. The decay rate of tail probability for unbounded and bounded pathloss functions is accurately captured for any fading distribution. While omitted for clarity, similar correspondence in instantaneous $(n = 1)$ and higher-order $(3 < n \leq L_{\max})$ joint tail probabilities was observed.

VI. Conclusion and Applications

In this paper, we derive the joint temporal statistics of interference in a decentralized wireless network with temporally correlated user locations. We show that joint interference statistics follow a multivariate Gaussian mixture distribution under the assumption of a bounded pathloss function. We also characterize the joint tail probability decay behavior for both bounded and unbounded pathloss functions. While the assumption of an unbounded pathloss function simplifies the derivation of joint interference statistics, it significantly overestimates the effect of interference on network performance measures. Thus the assumption of an unbounded pathloss function should be used with caution [8]. The distributions derived in this paper can be extended to include a slotted-ALOHA channel access protocol [14] in conjunction to the network model assumed in the paper. Extensions for contention based channel access protocols (such as CSMA), however, appears nontrivial [14] – but approximations may be proposed based on Poisson assumption with a Guard zone, that is analytically similar to the bounded pathloss function case [6].

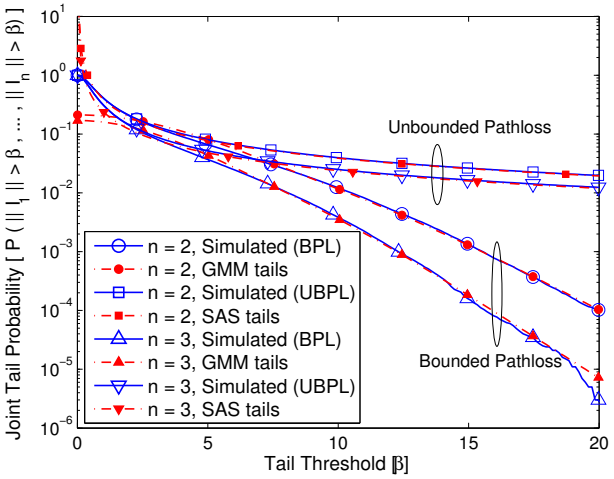

Fig. 2: Joint tail probability of interference over n time slots assuming both bounded (BPL) and unbounded (UBPL) pathloss functions in the presence of Rayleigh$\left(\frac{1}{\sqrt{2}}\right)$ fading. Simulated tail probabilities are compared against the estimated Gaussian mixture (GMM) and symmetric alpha stable (SAS) tails for BPL and UBPL, respectively. Empirical and estimated tail probabilities match closely for probability less than approximately 10^{-1}.

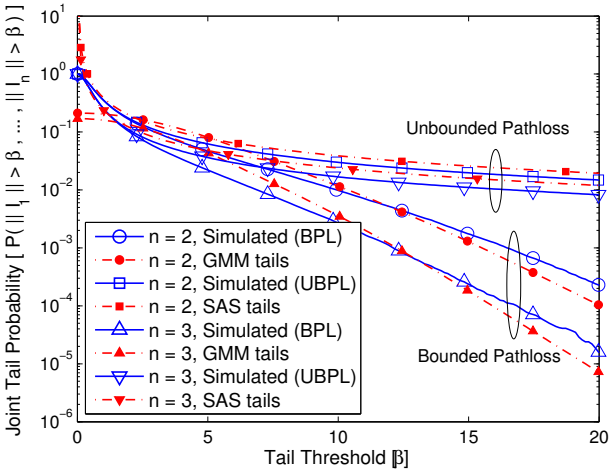

Fig. 3: Joint tail probability of interference over n time slots assuming both bounded (BPL) and unbounded (UBPL) pathloss functions in the presence of Nakagami$(0.5, 1)$ fading. The decay of the simulated tail probability matches the estimated Gaussian mixture (GMM) and symmetric alpha stable (SAS) tail decay for BPL and UBPL, respectively.

The closed-form interference statistics can be used to derive closed-form network performance measures that are asymptotically exact in the low outage regime [7], [14], [15]. Under the assumption of an unbounded pathloss function, this approach was used in [7] to derive closed-form single-hop communication performance measures, such as local delay, outage probability, and average network throughput. The closed-form expressions yielded up to $2\times$ improvement in network throughput by optimizing the lifetime distribution in view of the temporal correlations in the network [7]. Under the realistic assumption of a bounded pathloss function, the interference statistics derived in this paper can be used to revisit the analysis of [7] to further the accuracy of the results presented therein.

The closed-form interference statistics can also be used to design physical layer methods to improve the communication performance of receivers when treating interference as noise. The non-Gaussian interference statistics may severely degrade the communication performance of receivers that are designed assuming additive Gaussian noise in the system. The statistics of interference-plus-thermal-noise at the receiver governs the choice of the bit-error-rate optimal Bayesian detection rule, filtering structure, and more fundamentally, the distance measure (instead of the Gaussian optimal Euclidean norm) used to design the receiver [16], [17]. Prior papers have demonstrated 5–20dB gain in detection performance by using the optimal Bayesian detection rule, thereby improving the link spectral efficiency by several bps/Hz [16]–[19].

REFERENCES

[1] E. S. Sousa, "Performance of a spread spectrum packet radio network link in a Poisson field of interferers," *IEEE Transactions on Information Theory*, vol. 38, no. 6, pp. 1743–1754, Nov. 1992.

[2] J. Ilow and D. Hatzinakos, "Analytic alpha-stable noise modeling in a Poisson field of interferers or scatterers," *IEEE Transactions on Signal Processing*, vol. 46, no. 6, pp. 1601–1611, Jun. 1998.

[3] X. Yang and A. Petropulu, "Co-channel interference modeling and analysis in a Poisson field of interferers in wireless communications," *IEEE Transactions on Signal Processing*, vol. 51, no. 1, pp. 64–76, Jan. 2003.

[4] S. B. Lowen and M. C. Teich, "Power-law shot noise," *IEEE Transactions on Information Theory*, vol. 36, no. 6, pp. 1302–1318, Nov. 1990.

[5] M. Z. Win, P. C. Pinto, and L. A. Shepp, "A mathematical theory of network interference and its applications," *Proceedings of the IEEE*, vol. 97, no. 2, pp. 205–230, Feb. 2009.

[6] K. Gulati, B. L. Evans, J. G. Andrews, and K. R. Tinsley, "Statistics of co-channel interference in a field of Poisson and Poisson-Poisson clustered interferers," *IEEE Transactions on Signal Processing*, vol. 58, no. 12, pp. 6207–6222, Dec. 2010.

[7] K. Gulati, R. K. Ganti, J. G. Andrews, B. L. Evans, and S. Srikanteswara, "Characterizing decentralized wireless networks with temporal correlation in the low outage regime," *IEEE Transactions on Wireless Communications*, May 2011, accepted for publication. [Online]. Available: http://www.ece.utexas.edu/~bevans/papers/2012/decentralized/

[8] H. Inaltekin, S. B. Wicker, M. Chiang, and H. V. Poor, "On unbounded path-loss models: effects of singularity on wireless network performance," *IEEE Journal on Selected Areas in Communications*, vol. 27, no. 7, pp. 1078–1092, Sep. 2009.

[9] R. K. Ganti and M. Haenggi, "Spatial and temporal correlation of the interference in ALOHA ad hoc networks," *IEEE Communications Letters*, vol. 13, no. 9, pp. 631–633, Sep. 2009.

[10] M. Haenggi and R. K. Ganti, "Interference in large wireless networks," in *Foundations and Trends in Networking*. Now Publishers Inc., Dec. 2008, vol. 3, no. 2, pp. 127–248.

[11] D. Middleton, "Statistical–physical models of man–made and natural radio noise part II: First order probability models of the envelope and phase," U.S. Department of Commerce, Office of Telecommunications, Tech. Rep., Apr. 1976.

[12] G. Samorodnitsky and M. S. Taqqu, *Stable Non-Gaussian Random Processes: Stochastic Models with Infinite Variance*. Chapman and Hall, New York, 1994.

[13] R. Baldick, *Applied Optimization: Formulation and Algorithms for Engineering Systems*. Cambridge University Press, 2006.

[14] F. Baccelli and B. Błaszczyszyn, "Stochastic geometry and wireless networks, volume 2— applications," in *Foundations and Trends in Networking*. Now Publishers Inc., March 2009, vol. 4, no. 1–2, pp. 1–312.

[15] A. Rabbachin, T. Q. Quek, H. Shin, and M. Z. Win, "Cognitive network interference," *IEEE Transactions on Selected Areas in Communications*, vol. 29, no. 2, pp. 480–493, Feb. 2011.

[16] A. Spaulding and D. Middleton, "Optimum reception in an impulsive interference enviroment-part I: Coherent detection," *IEEE Transactions on Communications*, vol. 25, no. 9, pp. 910–923, 1977.

[17] W. Liu, P. P. Pokharel, and J. C. Principe, "Correntropy: Properties and applications in non-Gaussian signal processing," *IEEE Transactions on Signal Processing*, vol. 55, no. 11, pp. 5286–5298, 2007.

[18] D. Fertonani and G. Colavolpe, "A robust metric for soft-output detection in the presence of class-A noise," *IEEE Transactions on Communications*, vol. 57, no. 1, pp. 36–40, Jan. 2009.

[19] M. Nassar, K. Gulati, M. DeYoung, B. L. Evans, and K. R. Tinsley, "Mitigating near-field interference in laptop embedded wireless transceivers," *Journal of Signal Processing Systems*, Mar. 2009. [Online]. Available: http://dx.doi.org/10.1007/s11265-009-0350-7

Kapil Gulati (S'06 M'12) received the B.Tech. degree in Electronics and Communications Engineering from the Indian Institute of Technology, Guwahati in 2004 and the M.S. and Ph.D. degree in Electrical Engineering from the University of Texas at Austin in 2008 and 2011, respectively. From 2004 to 2006, he was employed as a Hardware Design Engineer at Texas Instruments, India. Since 2011, he has been employed as a Senior Systems Engineer at Qualcomm Incorporated, San Diego, CA.

Brian L. Evans (S'87, M'93, SM'97, F'09) is the Engineering Foundation Professor of Electrical and Computer Engineering at The University of Texas at Austin. He earned a BSEECS (1987) degree from the Rose-Hulman Institute of Technology, and MSEE (1988) and PhDEE (1993) degrees from the Georgia Institute of Technology. From 1993 to 1996, he was a post-doctoral researcher at the University of California, Berkeley.

Prof. Evans develops signal processing theory and algorithms with implementation constraints in mind, and translates algorithms into design methods, embedded prototypes and full system testbeds. He is currently researching interference mitigation in communication systems, rolling shutter artifact mitigation in video acquisition, and system-level reliability for multicore embedded systems.

He has published 200+ refereed conference and journal papers, and graduated 20 PhD students. He received several UT Austin teaching awards: ECE Lepley (2008), Texas Exes (2011) and IEEE/HKN Chapter Best Professor (2012). He received a 1997 US NSF CAREER Award.

Srikathyayani Srikanteswara is a Sr. Research Scientist at Intel Labs, where she leads research on cognitive radios and spectrum sharing techniques. She has been involved in shaping research on simultaneous operation of radios as well as developing and prototyping spectrum sensing algorithms. Prior to joining Intel, she was with Navsys Corporation, and Virginia Tech, where she was a research faculty member with the Mobile and Portable Radio Research Group (MPRG), where she developed Software Defined Radio (SDR) architectures for mobile platforms and DSP algorithms for communications. Her research interests include cognitive radios, multi radio interference mitigation, and spectrum sensing. She received her BS with Honors in Electrical Engineering from IT-BHU, India. She received MS and Ph.D. from Virginia Tech in 1997 and 2001 respectively.